www.nature.com/aps

Acta Pharmacologica Sinica

ARTICLE

Ursolic acid enhances autophagic clearance and ameliorates motor and non-motor symptoms in Parkinson's disease mice model

Yeojin Bang[1], Yoonjung Kwon[1], Mihyang Kim[1], Soung Hee Moon[1], Kiwon Jung[1] and Hyun Jin Choi[1]

Protein aggregation and the abnormal accumulation of aggregates are considered as common mechanisms of neurodegeneration such as Parkinson's disease (PD). Ursolic acid (UA), a natural pentacyclic triterpenoid compound, has shown a protective activity in several experimental models of brain dysfunction through inhibiting oxidative stress and inflammatory responses and suppressing apoptotic signaling in the brain. In this study, we investigated whether UA promoted autophagic clearance of protein aggregates and attenuated the pathology and characteristic symptoms in PD mouse model. Mice were injected with rotenone ($1\ mg \cdot kg^{-1} \cdot d^{-1}$, i.p.) five times per week for 1 or 2 weeks. We showed that rotenone injection induced significant motor deficit and prodromal non-motor symptoms accompanied by a significant dopaminergic neuronal loss and the deposition of aggregated proteins such as p62 and ubiquitin in the substantia nigra and striatum. Co-injection of UA ($10\ mg \cdot kg^{-1} \cdot d^{-1}$, i.p.) ameliorated all the rotenone-induced pathological alterations. In differentiated human neuroblastoma SH-SY5Y cells, two-step treatment with a proteasome inhibitor MG132 (0.25, 2.5 μM) induced marked accumulation of ubiquitin and p62 with clear and larger aggresome formation, while UA (5 μM) significantly attenuated the MG132-induced protein accumulation. Furthermore, we demonstrated that UA (5 μM) significantly increased autophagic clearance by promoting autophagic flux in primary neuronal cells and SH-SY5Y cells; UA affected autophagy regulation by increasing the phosphorylation of JNK, which triggered the dissociation of Bcl-2 from Beclin 1. These results suggest that UA could be a promising therapeutic candidate for reducing PD progression from the prodromal stage by regulating abnormal protein accumulation in the brain.

Keywords: autophagy; JNK; Parkinson's disease; rotenone; SH-SY5Y cells; ursolic acid

Acta Pharmacologica Sinica (2023) 44:752–765; https://doi.org/10.1038/s41401-022-00988-2

INTRODUCTION

Protein aggregation causes the abnormal accumulation and deposition of aggregates in specific cells and disturbances in their function. Neurons are among the most vulnerable cell types that encounter protein aggregate formation. Many studies have shown that the aggregation of misfolded proteins and their deposition in the brain are common pathogenic mechanisms of neurodegenerative diseases [1].

Emerging evidence shows that the aberrant regulation of protein clearance mechanisms is associated with the accumulation of protein aggregates and is closely related to the development of neurodegenerative disease. Macroautophagy (the main type of stress-induced autophagy, hereafter referred to as autophagy), a lysosome-dependent bulk degradation process, is an important mechanism required for maintaining cellular protein homeostasis in response to various stimuli, including nutrient deprivation, cellular injury, the abnormal accumulation of damaged organelles or membranes, and intracellular inclusions [2]. While nutrient deficiencies primarily regulate autophagy in most tissues, neuronal cells are sensitive to abnormally accumulated aggregates and react by inducing autophagy [3]. Ubiquitinated inclusions that are not sufficiently removed by the ubiquitin-proteasome system are further linked to p62 for autophagic degradation. Autophagic clearance is initiated by the formation of double-membrane structures called phagophores or pre-autophagosomal structures (PAS) that contain nearly 40 autophagy-related (Atg) proteins, including LC3-II. The phagophore progressively elongates and is enclosed to form an autophagosome. The mature autophagosome then fuses with a lysosome to form an autolysosome, within which the engulfed autophagic cargo is degraded.

The mammalian target of rapamycin (mTOR) signaling pathway is one of the best characterized pathways for autophagy regulation. AMP-activated protein kinase (AMPK) plays a crucial role in initiating autophagy by regulating mTOR phosphorylation. Beclin 1 has a core function in membrane trafficking and restructuring during autophagy through the formation of a core complex that contains the class III phosphatidylinositol-3 kinase (PI3KCIII) VPS34 [4]. Recent evidence has revealed that c-Jun N-terminal kinase (JNK) is essential for autophagy; specifically, JNK activation is essential for the regulation of *Atg* and *Beclin-1* transcription [5], p62 expression, and AMPK activation, and is involved in the post-transcriptional modification of Bcl-2, which could regulate autophagy [4].

Ursolic acid (UA; 3β-hydroxy-urs-12-en-28-oic acid) is a lipophilic, pentacyclic triterpenoid compound and is found in various plants

[1]College of Pharmacy and Institute of Pharmaceutical Sciences, CHA University, Pocheon, Gyeonggi-do 11160, South Korea
Correspondence: Hyun Jin Choi (hjchoi3@cha.ac.kr)

Received: 23 March 2022 Accepted: 22 August 2022
Published online: 22 September 2022

including *Rosmarinus officinalis* (rosemary) leaves, *Ocimum basilicum* (basil) leaves, *Coffea arabica* (coffee) leaves, and *Pyrus malus* (apple) peel. UA exhibits many pleiotropic biological activities, such as anti-tumoral, anti-diabetic, anti-inflammatory, antioxidant, and anti-hyperlipidemic properties [6]. Additionally, several studies using various cell models have recently reported evidence that UA regulates autophagy [7, 8]. UA induces cytotoxicity in cervical cancer cells through Atg-dependent autophagy activation and in human non-small cell lung cancer cells through JNK activation [9]. It also regulates uncoupling protein 1 and AMPK activities in adipose tissue, as well as protein kinase B and mTOR activities in muscle tissue [10]. In the central nervous system, UA has been reported to exert a protective effect against various brain dysfunctions, such as cognitive deficits, Parkinsonism [11, 12], brain hemorrhage, and cerebral ischemia [13]. Furthermore, it inhibits oxidative stress and inflammatory responses and suppresses apoptotic signaling in the brain [14]. However, it remains unclear whether UA regulates autophagy in the brain, where it could exert a crucial effect in inhibiting or attenuating neurodegenerative processes.

In this study, we aimed to investigate whether UA enhances autophagy-mediated protein clearance in neuronal cells and protects against protein aggregation-mediated cytotoxicity, as well as to determine which signaling pathway is relevant to such effects. For this, we used in vivo and in vitro experimental models representing protein aggregates in neuronal cells and related pathology. We found that UA exerts neuroprotective effects both in vivo and in vitro, ameliorates Parkinson's disease (PD)-like motor and non-motor signs, and attenuates protein accumulation in neuronal cells. Moreover, UA induces autophagy-mediated protein clearance by activating the JNK signaling pathway and destabilizing the Bcl-2–Beclin 1 complex.

MATERIALS AND METHODS

Materials

Dulbecco's modified Eagle's medium (DMEM), fetal bovine serum (FBS), penicillin/streptomycin, and trypsin/EDTA were purchased from Corning (Corning, NY, USA). MG132 was obtained from Enzo Life Sciences, Inc. (Farmingdale, NY, USA), and protease inhibitor cocktail and phosphatase inhibitor cocktail were obtained from Roche (Basel, Switzerland). Alexa Fluor conjugated secondary antibody, 4′,6-diamidino-2-phenylindole dilactate (DAPI), and ProLong Gold antifade reagent were purchased from Invitrogen (Waltham, MA, USA). All other chemicals were of reagent grade and were purchased from Sigma-Aldrich (St. Louis, MO, USA).

Animals and treatment

Eight-week-old male C57BL/6 mice weighing 20–25 g were purchased from Orient Bio Inc. (Seongnam, South Korea). G2019S-leucine-rich repeat kinase 2 (LRRK2)-Tg FVB mice expressing a high copy number of mutant human LRRK2 with a Gly2019Ser substitution were purchased from Jackson Laboratory [15] (stock #009609; Bar Harbor, ME, USA). G2019S-LRRK2 female mice were crossed with background-matched FVB wild-type male mice, and the selective breeding preserved the transgene in the hemizygous state. Genotyping was carried out according to the manufacturer's instructions (Jackson Laboratory). The experiments were performed in the specific-pathogen-free laboratory animal room of CHA University. All animals were maintained in cages under standard conditions at 22 ± 2 °C with 60% relative humidity and exposed to a 12-h light/dark cycle with food and water available ad libitum. Mice were housed with no more than five animals per cage.

Experimental design

To examine the effect of UA on rotenone-induced PD pathology, 48 mice were randomly divided into six groups ($n = 8$ per group): the control (1 week), rotenone (1 mg/kg, 1 week), rotenone + UA (10 mg/kg, 1 week), control (2 weeks), rotenone (1 mg/kg, 2 weeks), and rotenone + UA (10 mg/kg, 2 weeks) groups. Rotenone was dissolved in 1% polyethylene glycol and 0.2% dimethyl sulfoxide (DMSO) immediately before use and injected at a volume of 5 μL/g body weight through a single intraperitoneal (ip) injection at a dose of 1 $mg \cdot kg^{-1} \cdot d^{-1}$, five times per week for 1 or 2 weeks. UA was dissolved in 4% DMSO and injected at 5 μL/g body weight via a single ip injection at 10 $mg \cdot kg^{-1} \cdot d^{-1}$.

Behavioral tests

Locomotor activity and motor coordination. Spontaneous locomotor activity was tested based on the open field test [16]. Each mouse was placed individually in the center of the open field (50 cm × 50 cm), and a video was recorded for 10 min [17]. The analysis was performed using a computerized tracking system (EthoVision XT 9.0; Noldus, Netherlands). The automatically analyzed locomotor variables were as follows: total distance moved, total distance covered by the animals during the entire 10-min observation period (in cm). Motor coordination was assessed using the rotarod test (JD-A-07MA5; Jeungdo B & P Co. Ltd., Seoul, South Korea). All test animals received adaptive training at 4 rpm for 3 min before the test. The mouse latency to fall was recorded over three consecutive trials at a rotation speed ranging from 4 to 40 accelerating rpm for a maximum of 5 min. Each experiment was independently evaluated by two experimenters blinded to the drug treatments.

Depressive-like behavior; Forced swim test (FST). Each mouse was placed in a glass cylinder (25 cm in height and 13 cm in diameter), which was filled up to 15 cm with water at 25 °C, and allowed to swim. A video was recorded for 10 min. After the end of the test, the mouse was gently dried and placed under a warm light for 10 min. The immobility time was determined [18]. Each experiment was independently evaluated by two experimenters blinded to the drug treatments.

Cell culture and treatment

Human neuroblastoma SH-SY5Y cells were grown in DMEM containing 10% FBS, 100 IU/L penicillin, and 10 μg/mL streptomycin at 37 °C in 5% CO_2 and 95% air in a humidified atmosphere. The cells were differentiated for 3 days with 10 μM all-trans-retinoic acid and 1% FBS in DMEM.

Primary cortical neuron cultures were isolated from embryonic day (E) 18 C57BL/6 mouse embryos [19]. Briefly, E18 mouse embryos were dissected and maintained in ice-cold Hank's balanced salt solution and then dissociated in StemPro Accutase Cell Dissociation Reagent (Thermo Fisher Scientific Cat# A1110501) for 10 min in a 37 °C water bath. The dissociated cells were then washed twice by adding Hank's balanced salt solution, allowing the tissue to settle to the bottom of the tube, and the Hank's balanced salt solution supernatant was carefully aspirated. The cells were triturated using a fire-polished Pasteur pipet with C-NBM (neurobasal media containing 2% B-27, 1% glutamate, and 1% penicillin/streptomycin), plated at an appropriate density, and subsequently maintained in a humidified CO_2 incubator for 4 h at 4 °C, followed by renewal with fresh media. Half of the cell medium was replaced with C-NBM every 2 days.

Primary dopaminergic neurons from E13.5 C57BL/6 mouse embryos were dissected and separated, as with the cortical neurons. They were then maintained in a humidified CO_2 incubator for 24 h at 4 °C, followed by renewal with fresh media. The cell medium was replaced with C-NBM every day. Primary neurons were used for the in vitro experiments between days 7 and 10.

In vitro two-step MG132 treatment

Differentiated SH-SY5Y cells were pre-incubated with a low concentration of MG132 (0.25 μM) in differential media (10 μM retinoic acid and 1% FBS in DMEM). After 24 h, the cells were incubated in normal media (10% FBS in DMEM) for 8 h and

subsequently treated with a high concentration of MG132 (2.5 μM) for an additional 16 h [20].

Cell death assay
The extent of cell death was assessed by measuring the amount of lactate dehydrogenase released into the culture medium using a previously described method [20]. The absorbance was measured at 490 nm using a microplate spectrophotometer (VersaMax; Molecular Devices, CA, USA), and all values were normalized by comparison with the vehicle control.

NP-40-soluble and sodium dodecyl sulfate (SDS)-soluble fractions
Cells were lysed in NP buffer (150 mM NaCl, 1% NP-40, 1 mM EDTA, 5% glycerol, and 25 mM Tris–Cl; pH 7.5) with a protease inhibitor cocktail and phosphatase inhibitor cocktail (Roche) for 2 h at −80 °C. Cell lysates were centrifuged at 12,000 × *g* for 60 min at 4 °C, and supernatant proteins, the NP-soluble fraction, were collected. The pellet was further lysed in SDS buffer (2% SDS and 50 mM Tris–Cl, pH 7.5) using a protease inhibitor cocktail and phosphatase inhibitor cocktail sonicated for homogenization and then boiled at 100 °C for 5 min. The SDS-soluble fraction was collected by centrifugation at 12,000 × *g* for 60 min at 4 °C. Protein samples were subjected to SDS-PAGE and immunoblotted as described as described hereunder.

Western blot analysis
To prepare for the Western blot analysis, cells were washed with ice-cold phosphate-buffered saline (PBS), harvested, and lysed in radioimmunoprecipitation assay buffer (150 mM NaCl, 1% NP-40, 0.5% deoxycholic acid, 0.1% SDS, and 50 mM Tris–Cl; pH 7.5) with complete protease inhibitor cocktail and phosphatase inhibitor cocktail (Roche) for 30 min. Cell lysates were centrifuged at 12,000 × *g* for 30 min at 4 °C. Supernatant proteins were collected and quantified using the Bradford protein assay reagent (Bio-Rad Laboratories, Inc., Hercules, CA, USA). Equal amounts of protein were separated by 8%–12% SDS-PAGE gels and transblotted onto polyvinylidene difluoride-nitrocellulose membranes. Membranes were blocked using 5% skim milk in Tris buffered saline with Tween 20 and incubated at 4 °C overnight using the following primary antibodies: mouse anti-tyrosine hydroxylase (TH) (Santa Cruz Biotechnology Inc. Cat# sc-25269, 1:5000), mouse anti-p62/SQSTM1 (Santa Cruz Biotechnology Inc. Cat# sc-28359, 1:2000), rabbit anti-phospho-AMPKα1/2 (Thr172) (Santa Cruz Biotechnology Inc. Cat# sc-33524, 1:1000), mouse anti-ubiquitin (Santa Cruz Biotechnology Inc. Cat# sc-8017, 1:5000), mouse anti-Bcl-2 (Santa Cruz Biotechnology Inc. Cat# sc-7382, 1:2000), rabbit anti-mTOR (Cell Signaling Technology, Danvers, MA, USA; Cat# 2972, 1:1000), rabbit anti-phospho-mTOR (Ser2448) (Cell Signaling Technology, Cat# 2971, 1:1000), rabbit anti-Akt (Cell Signaling Technology, Cat# 9272, 1:1000), rabbit anti-phospho-Akt (Ser473) (Cell Signaling Technology, Cat# 9271, 1:1000), rabbit anti-SAPK/JNK (Cell Signaling Technology, Cat# 9252, 1:1000), rabbit anti-phospho-SAPK/JNK (Thr183/Tyr185) (Cell Signaling Technology, Cat# 9251, 1:1000), rabbit anti-Beclin-1 (Cell Signaling Technology, Cat# 3738, 1:2000), rabbit anti-LC3 (Novus Biologicals, Littleton, CO, USA; Cat# NB-600-1384, 1:5000), rabbit anti-p62/SQSTM1 (Sigma-Aldrich, Cat# P0067, 1:5000), rabbit anti-GAPDH (Sigma-Aldrich, Cat# G9545 1:5000), and mouse anti-β-actin (Sigma-Aldrich, Cat# A1978, 1:10000). Each membrane was then blotted with the following horseradish peroxidase-conjugated secondary antibodies: goat anti-rabbit IgG (Thermo Fisher Scientific, Cat# 31460) and goat anti-mouse IgG (Thermo Fisher Scientific, Cat# 31430). Proteins were detected using enhanced chemiluminescence (Millipore-Sigma, Burlington, MA, USA) and analyzed with a LAS-4000 luminescent image analyzer (Fujifilm, Tokyo, Japan). The relative intensities of each band were measured using Multi-Gauge Software (Fujifilm) and normalized to GAPDH or β-actin.

Immunohistochemistry
At the end of the experiments, mice were deeply anesthetized using a 4:1 mixture of alfaxalone and xylazine and transcardially perfused using PBS and ice-cold 4% paraformaldehyde. Brain tissue samples for immunohistochemistry were prepared as paraffin-embedded tissue. Brains were collected and post-fixed in 4% paraformaldehyde for 24 h and subsequently transferred to a 15% sucrose solution and kept in a 30% sucrose solution at 4 °C before being sliced in coronal sections (20 μm-thick) using a cryostat (Leica DM750; Leica, Wetzlar, Germany). Brain slices were kept in a cryoprotectant solution at 4 °C until further processing. The slices were incubated overnight using the following primary antibodies: rabbit anti-TH (Abcam, Cambridge, UK; Cat# ab112, 1:2000), mouse anti-ubiquitin (1:200), rabbit anti-p62/SQSTM1 (1:200), and rabbit anti-LC3 (1:1000) diluted in 0.05 M PBS and 1.5% normal goat serum. After washing, the slices were incubated with biotinylated goat anti-rabbit (Vector Laboratories, Inc., Burlingame, CA, USA; Cat# BA1000, 1:400) or goat anti-mouse IgG (Vector Laboratories, Inc. Cat# BA9200, 1:400) secondary antibody for 1 h at room temperature (RT). To visualize staining, the Vectastain Elite ABC Kit and DAB Kit (Vector Laboratories, Inc.) were used, and samples were mounted onto gelatin-coated slides under Vectashield mounting medium. Bright-field images were collected using a Leica DM750 (Leica). Immunoreactivity was measured by semi-quantitative densitometric analysis using NIH-produced software (ImageJ win64 Fiji). Pearson's correlation coefficient was calculated using the co-localization plugin of ImageJ. The analysis was blinded.

Immunoprecipitation
Immunoprecipitation was carried out using a Classic IP kit (Thermo Fisher Scientific) according to the manufacturer's instructions. Briefly, total proteins were extracted and quantified. A total of 500 μg protein in 300 μL of supernatant was incubated with 5 μg anti- Beclin-1 antibody under rotation overnight at 4 °C. The protein A/G agarose was washed, eluted in sample buffer, and boiled for 10 min at 100 °C. The immune complexes were subjected to Western blot analysis as described previously herein using the indicated primary antibodies.

Immunofluorescence confocal microscopy
SH-SY5Y cells and primary cortical neurons were plated on poly-*D*-lysine-coated cover slips in 12-well culture plates. Primary dopaminergic neurons were plated on poly-*L*-ornithine-coated cover slips in 12-well culture plates. After the individual experiments, the cells were washed with PBS and fixed for 15 min in cold 4% paraformaldehyde, 4% sucrose, and 1% BSA in PBS (pH 7.4). Thereafter, the cells were permeabilized with 0.25% Triton-X-100 in PBS for 10 min and subsequently blocked with PBS containing 1% BSA, 1% normal goat serum, and 3% FBS for 30 min at RT to reduce non-specific binding. Thereafter, cells were incubated overnight using the following primary antibodies: mouse anti-TH (1:200), rat anti-DA transporter (DAT) (Santa Cruz Biotechnology Inc. Cat# sc-32258, 1:100), mouse anti-LAMP-2 (Santa Cruz Biotechnology Inc. Cat# sc-18822, 1:100), mouse anti-α-tubulin (Santa Cruz Biotechnology Inc. Cat# sc-5286, 1:800), rabbit anti-βIII tubulin (Abcam, Cat# ab18207, 1:1600), and rabbit anti-LC3 (1:1600) in PBS containing 1% BSA at 4 °C. Subsequently, the cells were incubated with the following secondary antibodies: goat anti-mouse IgG Alexa Fluor 568 (Invitrogen, Cat# A11004), goat anti-rabbit IgG Alexa Fluor 647 (Invitrogen, Cat# A32733), goat anti-rabbit IgG Alexa Fluor 488 (Invitrogen, Cat# A11008), goat anti-mouse IgG Alexa Fluor 488 (Invitrogen, Cat# A32723), goat anti-rat IgG, Alexa Fluor 594 (Invitrogen, Cat# A48264), and Alexa Fluor 555 phalloidin (Invitrogen, Cat# A34055) for 50 min at RT, following which DAPI was added for 10 min. Phalloidin was used for F-actin staining.

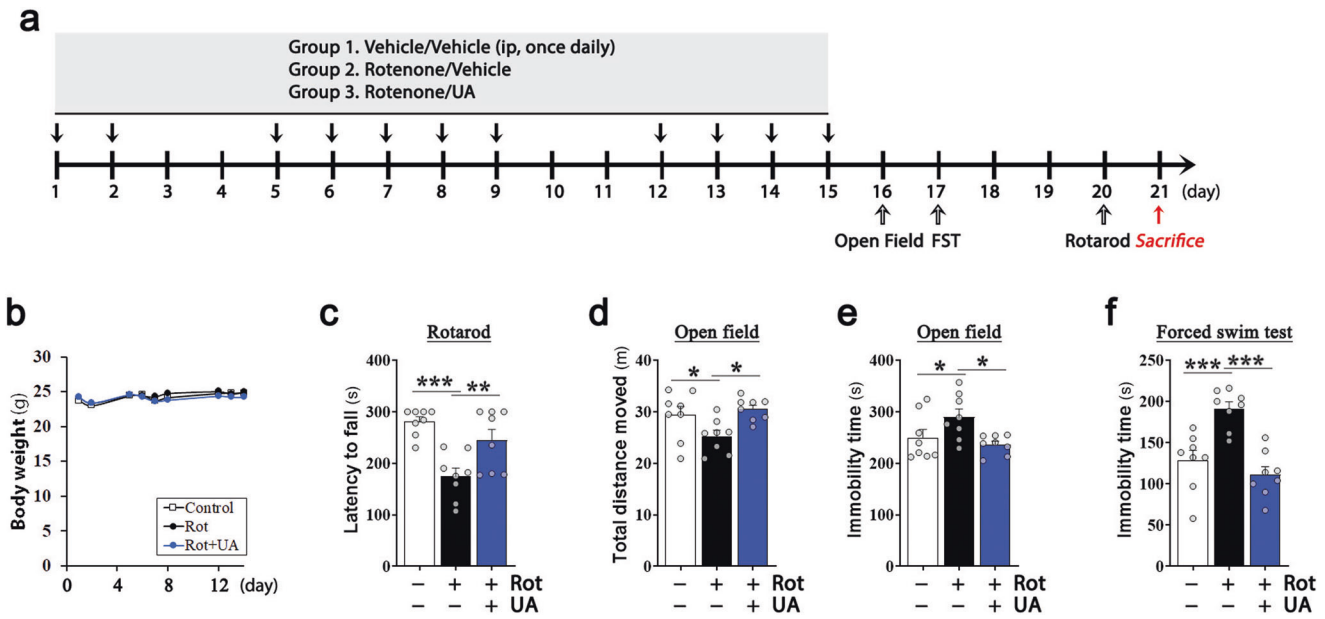

Fig. 1 Effect of ursolic acid (UA) on the behavior of rotenone-induced Parkinson's disease model mice. a Scheme of the experimental procedure for 2 weeks of treatment. **b** Body weight assessed over the 2 weeks of treatment. **c** Latency to fall (s) in the accelerating rotarod 5 days after the last injection. **d** Total distance moved (m) and **e** immobility time (s) in the open field test, measured for 10 min, 1 day after the last injection. **f** Immobility time (s) in forced swim test 2 days after the last injection. Data are expressed as mean ± SEM. $n = 8$ mice per group, $^{*}P < 0.05$; $^{**}P < 0.01$; $^{***}P < 0.001$ according to one-way ANOVA followed by the post hoc Holm–Sidak test. FST forced swim test, ip intraperitoneal, Rot rotenone.

Images were captured using LSM880 confocal laser scanning microscopes (Zeiss, Jena, Germany). The paired images in all figures were obtained at the same gain and offset settings. The number of spots, amount of co-localization, and neurite lengths were measured using ImageJ. Neurites stained with βIII tubulin or TH were traced and scored to determine the total neurite length per cell. The total neurite length per neuron was measured using the Skeleton plugin of ImageJ. For quantitative analysis, 6–10 images for each experimental condition were obtained from each coverslip. The analysis was blinded.

Data and statistical analysis

Statistical analysis was undertaken only for studies where each group size was at least $n = 5$. All group sizes represent the number of experimental independent values, and these independent values were used to evaluate statistical analyses. Two-group comparisons were carried out using Student's *t* test or the Wilcoxon matched-pairs signed rank test [21], and multiple comparisons were analyzed by one or two-way ANOVA followed by the post hoc Holm–Sidak test or Dunn's multiple comparisons test. The statistical tests used are indicated in the figure legends. Post hoc tests were conducted only if the *F* statistic from ANOVA achieved $P < 0.05$ and there was no inhomogeneity of variance. Data are expressed as mean ± SEM. To reduce unwanted sources of variation, data normalization was performed. For the results of the cell death assay and immunohistochemistry, each value was divided by the mean of the indicated group (100%), whereas Western blot data were subjected to non-parametric statistical analysis. All statistical analyses were performed using GraphPad Prism version 8.0.2 for Windows (GraphPad Software, San Diego, CA, USA). $P < 0.05$ was considered statistically significant.

RESULTS

UA ameliorates motor and non-motor dysfunction in rotenone-treated mice

Rotenone is widely used to reproduce many aspects of the pathology of human PD [22]. Rotenone induces PD-like motor and non-motor signs, with nigrostriatal dopaminergic neurodegeneration and the accumulation of protein aggregates in the brain [23]. In order to reproduce non-motor prodromal symptoms including depression more clearly, we injected a much lower dose (1 mg/kg, once daily) of ip rotenone for 2 weeks than the amount that normally causes motor deficiency (2.5 mg/kg, once daily). Our previous study showed that 1 mg/kg of rotenone-injected daily for 2 weeks also induced a PD-like pathology including motor deficits and TH-positive neuronal loss in the substantia nigra pars compacta (SNpc) [24]. To investigate whether UA ameliorates PD signs and pathology in rotenone-treated mice, we sequentially injected UA (10 mg/kg, i.p., once daily, 5 days per week) and rotenone (5 days per week) into C57BL/6 mice for 2 weeks and performed behavioral tests (Fig. 1a). There were no significant differences in mortality and body weights between the experimental groups (Fig. 1b).

Motor function in mice was evaluated using the rotarod and open field tests. Rotenone exposure for 2 weeks caused a significant decrease in the latency to fall in the rotarod test (Fig. 1c). However, UA significantly improved the motor coordination of rotenone-injected mice as compared with that in the group treated with rotenone alone. This result was further verified by an open field test, as shown in Fig. 1d. The total distance traversed by the mice was decreased in the rotenone-treated group; this was ameliorated by co-treatment with UA. Additionally, rotenone caused a significant decrease in the locomotor activity of mice in the open field test but not in those co-treated with UA (Fig. 1e). The changes in the immobility time in the open field test could be suggestive of depression-like behavior, and therefore, we further evaluated whether UA could improve rotenone-induced non-motor behavioral changes using the FST. Immobility time during the FST was significantly increased in the rotenone-treated mice, which was suggestive of depressive behavior, and was attenuated by UA co-treatment (Fig. 1f). As non-motor signs are considered prodromal indicators that typically precede the motor disease signs of PD, we sought to assess whether rotenone-induced non-motor dysfunction could be detected in mice after 1 week of

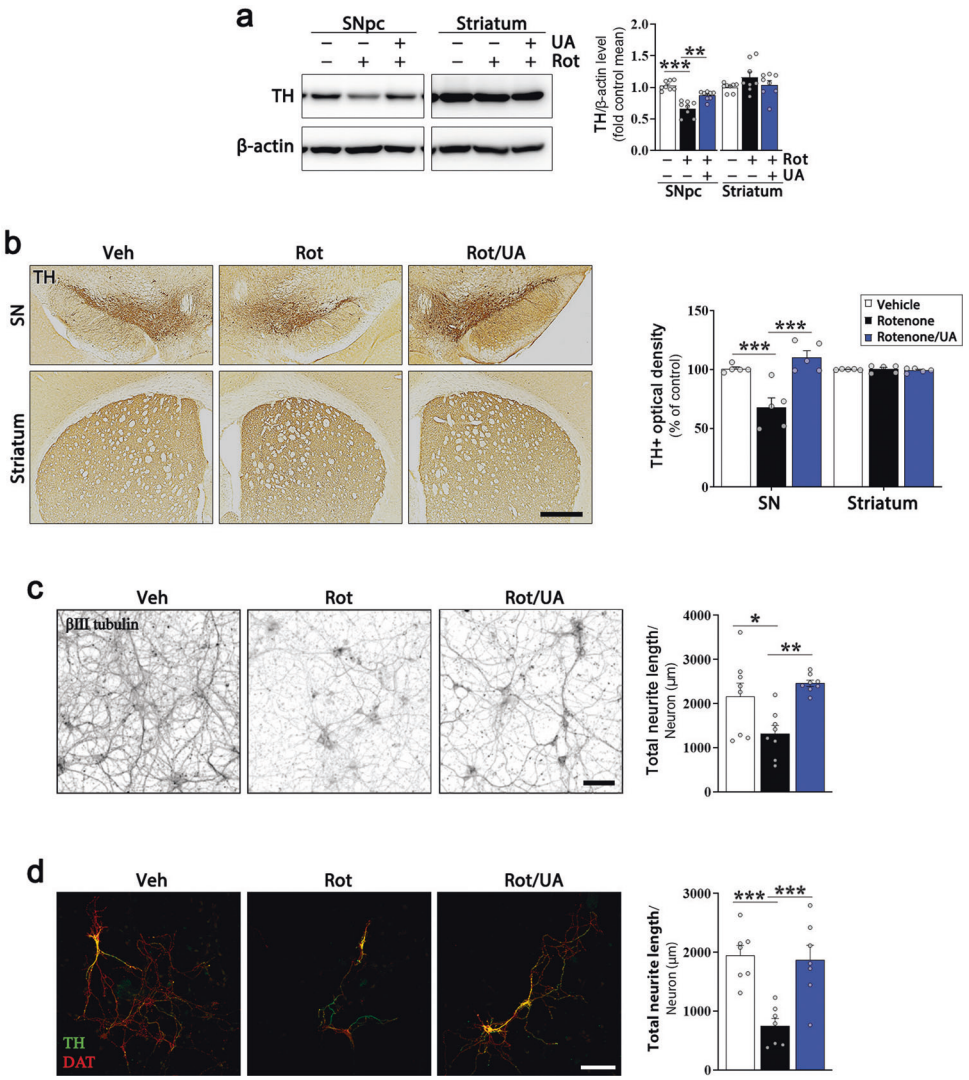

Fig. 2 Effects of ursolic acid (UA) on rotenone-induced neuronal loss. a The substantia nigra pars compacta (SNpc) and striatum were extracted from a subset of mice from each group and analyzed for tyrosine hydroxylase (TH) protein expression. Right, quantification of TH/β-actin; $n = 8$; two-way ANOVA followed by the post hoc Holm–Sidak test. **b** Representative light microphotographs of TH immunostaining in the substantia nigra (SN) (top) and striatum (bottom) of mouse brains; scale bar = 500 μm. Right, quantitation of optical densities of TH-positive neurons; $n = 5$; two-way ANOVA followed by the post hoc Holm–Sidak test. **c** Immunofluorescence staining of βIII tubulin in primary cortical neurons treated with 5 nM rotenone with or without 5 μM UA for 2 days; scale bar = 100 μm. Right, quantitation of total neurite length of βIII tubulin-positive neurons; $n = 8$; one-way ANOVA followed by the post hoc Holm–Sidak test. **d** Immunofluorescence staining of TH and DA transporter (DAT) in dopaminergic primary neurons treated with 5 nM rotenone with or without 5 μM UA for 2 days; scale bar = 100 μm. Right, quantitation of total neurite length of TH-positive neurons; analyzed by one-way ANOVA followed by the post hoc Holm–Sidak test. The paired images were obtained at the same gain and offset settings. Data are expressed as mean ± SEM. $^{*}P < 0.05$; $^{**}P < 0.01$; $^{***}P < 0.001$. Rot rotenone, Veh vehicle.

exposure. The mice exposed to rotenone for 1 week tended to exhibit depressive behaviors in the FST and tail suspension test, similar to that observed in the mice treated for 2 weeks, although there were no statistically significant differences (Supplementary Fig. S1). Anosmia, another prodromal sign of PD, was also detected in mice treated with rotenone for 1 week based on the buried pellet test. Interestingly, both depressive behavior and olfactory dysfunction were ameliorated by UA. Altogether, these findings indicate that UA improves rotenone-induced PD-like motor and non-motor disease signs.

UA is protective against rotenone-induced neuronal cell death

We next examined whether UA exhibits protective effects against rotenone-induced dopaminergic (DAergic) neurodegeneration in the SNpc and the striatum of the mouse brain. We analyzed TH levels as an indicator of DAergic neuronal loss. Significantly decreased TH protein levels were detected in the SNpc of rotenone-treated mice, and this was attenuated by UA (Fig. 2a). There were no significant changes in the TH levels in the striatum between experimental groups. These results were further confirmed by immunohistochemistry against TH in the same regions (Fig. 2b).

To verify the neuroprotective activity of UA in vitro, we used two primary culture systems, a mouse cortical neuronal culture and midbrain DAergic neuronal culture. Immunofluorescence analysis of βIII tubulin revealed that rotenone reduced both the numbers and lengths of neurites of primary cortical neurons, and this was ameliorated by the presence of UA (Fig. 2c). Furthermore, UA was also protective against rotenone-induced degeneration of TH-positive and DAT-positive primary DAergic neurons (Fig. 2d).

Therefore, all these results indicate the neuroprotective effect of UA on rotenone-induced neuronal loss.

UA attenuates the accumulation of aggregated proteins in neuronal cells

Since the accumulation of protein aggregates is a relatively early pathogenic event in neurodegeneration [25], we next assessed whether rotenone-induced neurotoxicity is associated with protein accumulation and whether UA regulates the rotenone-induced accumulation of protein aggregates in the brain. In our previous study, we reported a significant increase in protein aggregates in the brain, which was detected prior to motor dysfunction after 1 week of rotenone treatment, and was associated with the prodromal non-motor signs in a rotenone-induced PD mouse model [24]. Therefore, we examined the effect of UA on the immunoreactivities of ubiquitin and p62 in the SNpc, striatum, and cortex of rotenone-exposed mice for 1 week. These proteins are essential in the delivery of ubiquitinated cargo for autophagy-mediated degradation and are detected as cytoplasmic inclusions of the brain in patients with neurodegenerative disease [26]. Rotenone increased the immunoreactivity of ubiquitin (Fig. 3a) and p62 (Fig. 3b) in the SNpc, striatum, and cortex of mice, and this was attenuated by UA. The most significant change in protein accumulation was detected by quantification of the p62-positive area.

The effect of UA on the accumulation of protein aggregates in neuronal cells was also evaluated in proteasome inhibitor MG132-treated neuroblastoma SH-SY5Y cells. We previously showed that sequential treatment with lower and higher concentrations of MG132 causes protein accumulation with clear and larger aggresome formation [27, 28]. UA attenuated the MG132-induced accumulation of ubiquitin and p62 in differentiated SH-SY5Y cells (Fig. 3c). These data indicate that UA can regulate the accumulation of protein aggregates in neuronal cells.

UA activates both autophagy induction and turnover

To verify whether activation of autophagy is responsible for the UA-induced attenuation of neuronal loss and protein accumulation in the brain of rotenone-treated mice, we next examined the effect of UA on autophagy induction and turnover. UA increased the immunoreactivity of LC3, a standard marker of autophagosomes, in the SNpc, striatum, and cortex of mice (Fig. 4a). In primary cortical neurons (Fig. 4b) and differentiated SH-SY5Y cells (Fig. 4c), UA significantly upregulated LC3-II protein levels, suggesting the induction of autophagy. To further evaluate the effects of UA on autophagy processes, such as fusion between the autophagosome and lysosome or the accumulation of autolysosomes, we examined the intracellular localization of LC3 and LAMP-2A in control and UA-treated SH-SY5Y cells. In UA-treated cells, LC3 immunoreactivity was increased, redistributed to autophagic vacuoles, and colocalized with LAMP-2A, indicating autolysosome formation through fusion between the autophagosome and lysosome (Fig. 4d). To confirm that the increase in LC3-II protein levels by UA was due to the induction of autophagy and not due to the disruption of autophagic turnover, we compared UA-induced increases in LC3-II between cells treated with or without the autophagy flux inhibitor NH_4Cl. NH_4Cl interferes with the fusion of autophagosomes with lysosomes, thereby blocking the degradation of the autolysosome, and causing the accumulation of LC3-II in the autolysosome [29]. Co-treatment with NH_4Cl and UA (5 μM, 3.746 ± 0.069) resulted in significant increases in LC3-II levels compared with those treated with UA alone (2.832 ± 0.497) or NH_4Cl alone (2.599 ± 0.299) (Fig. 4e).

As several studies have demonstrated increased LC3 expression and accumulation of autophagic vacuoles in rotenone-treated PD models [30], we measured the immunoreactivity of LC3 and ubiquitin in the cortex of rotenone-treated mice (Fig. 5a). The LC3 immunoreactivity tended to increase in the cortex of rotenone-treated mice, and this increase was greater in the presence of UA. Interestingly, the Pearson's correlation coefficients of ubiquitin and LC3, which suggest their co-localization, were significantly increased due to UA treatment than in mice treated with rotenone alone. These results indicate that the accumulation of LC3 in rotenone-treated mice brains is caused by impaired autophagic degradation, as previously reported in rotenone-treated PD model brains [31, 32]. Furthermore, we investigated whether UA could ameliorate rotenone-induced decrease in autophagic degradation. For this, differentiated SH-SY5Y cells were treated with rotenone in the presence or absence of UA, and the intensities and intracellular distribution patterns of LC3 puncta and p62 aggregates were evaluated (Fig. 5b). As observed in the cortex of the rotenone-treated mice (Fig. 5a), increase in the LC3 immunoreactivity was detected in both cells treated with rotenone alone as well as those treated with rotenone and UA. Additionally, the number of LC3 and p62 co-localization puncta was also increased in both treatment conditions. Furthermore, the p62 immunoreactivity significantly increased in cells treated with rotenone alone, but reduced in the presence of UA. In cells treated with rotenone and UA, most of p62 was found to colocalize with LC3, whereas in cells treated with rotenone alone, the co-localization ratio of p62 and LC3 was low. Overall, these results indicate that rotenone causes an accumulation of autophagic vacuoles by disrupting their lysosomal degradation, and UA induces autophagy and the subsequent autophagic clearance.

JNK activation is involved in UA-mediated induction of autophagy

To identify the signaling pathways underlying UA-mediated induction of autophagy, we examined the effect of UA on PI3K/Akt/mTOR signaling, which is a well-known regulatory pathway of autophagy [33]. There were no significant changes in p-mTOR or p-Akt levels up to 4 h after UA treatment, even though a significant increase in LC3-II was observed under the same conditions (Fig. 6a).

Several studies have demonstrated that UA can activate the JNK pathway and regulate cell viability and functions [9]; therefore, we investigated whether the this pathway was involved in UA-induced autophagy in neuronal cells. Activated JNK phosphorylates Bcl-2, which leads to the dissociation of Bcl-2 from Beclin 1 and the formation of the PI3KCIII/Vps34/Beclin 1 complex, followed by autophagosome synthesis [34]. In this study, UA significantly increased phosphorylation of JNK (p54 and p36) as early as 1 h after treatment (Fig. 6b). The immunoprecipitation results indicated that the interactions between Beclin 1 and Bcl-2 were decreased in UA-treated cells (Fig. 6c). The specific JNK inhibitor SP600125 attenuated the UA-induced phosphorylation of JNK and increase in LC3-II (Fig. 6d, e). These results suggest that UA induced autophagy via the JNK-dependent dissociation of Bcl-2 from Beclin 1 (Fig. 7e).

As AMPK promotes autophagy by inhibiting mTOR complex 1 (mTORC1) or activating JNK [35], we further examined whether the energy sensor AMPK was activated by UA and was involved in UA-mediated induction of autophagy. In this study, the phosphorylation of AMPK was increased by UA at an early time point (Supplementary Fig. S2a). However, compound C, an AMPK inhibitor, did not affect the phosphorylation of JNK or the protein level of LC3-II (Supplementary Fig. S2b, c). These results suggest that AMPK is activated by UA but not involved in the UA-mediated regulation of autophagy function. Autophagy could be regulated by both class I and class III PI3Ks; PI3KCIII/Vps34/Beclin 1 promotes autophagy as a downstream mediator of JNK, but class I PI3K/Akt/mTOR negatively regulates autophagy as an upstream modulator of JNK [36]. Interestingly, the PI3K inhibitor 3-methyladenine (3-MA) attenuated the UA-induced increase of LC3-II, similar to the effect of SP600125, but did not affect the phosphorylation of JNK (Supplementary Fig. S2b, c). These data suggest that PI3KCIII is activated by UA and is involved in the induction of autophagy.

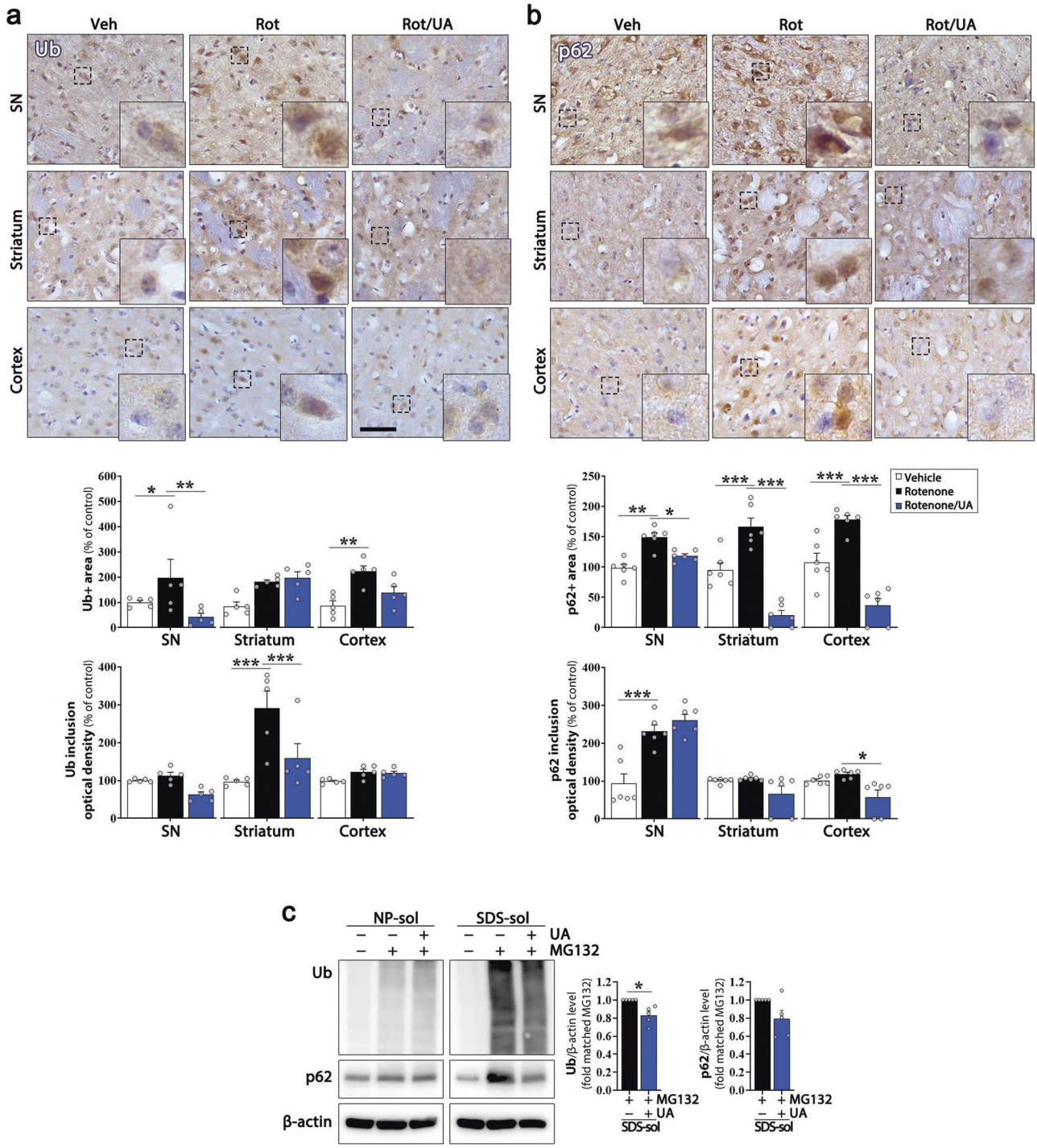

Fig. 3 Effects of ursolic acid (UA) on the accumulation of ubiquitin (Ub) and p62 protein inclusions. a, **b** Immunostaining for Ub (**a**; $n = 5$) and p62 (**b**; $n = 6$) in the substantia nigra (SN), striatum, and cortex of mouse brains injected with rotenone with or without UA for 1 week; scale bar = 50 μm. Bottom, quantification of Ub or p62-positive areas and optical density. Two-way ANOVA followed by the post hoc Holm–Sidak test. **c** Western blot analysis of NP-soluble and SDS-soluble fractions of Ub and p62 protein levels in SH-SY5Y cells treated with two-step MG132 and UA; scale bar = 100 μm. Right, quantification of the Ub and p62/β-actin protein levels; $n = 5$; Wilcoxon matched-pairs signed rank test. The paired images were obtained at the same gain and offset settings. Data are expressed as mean ± SEM. $^{*}P < 0.05$; $^{**}P < 0.01$; $^{***}P < 0.001$. Rot rotenone, SDS sodium dodecyl sulfate, sol soluble, Ub ubiquitin, Veh vehicle.

UA is neuroprotective via JNK-dependent induction of autophagy To verify whether JNK-dependent induction of autophagy plays a crucial role in the neuroprotective effect of UA, we examined the neuroprotective effect of UA against rotenone in the presence or absence of SP600125 or 3-MA in primary cortical neurons and DAergic neurons. Rotenone-induced decreases in βIII immunoreactivity in primary cortical neurons (Fig. 7a) as well as TH and DAT immunoreactivities in primary DAergic neurons (Fig. 7b) were significantly attenuated by UA. Both SP600125 and 3-MA interfered with the neuroprotective activity of UA in

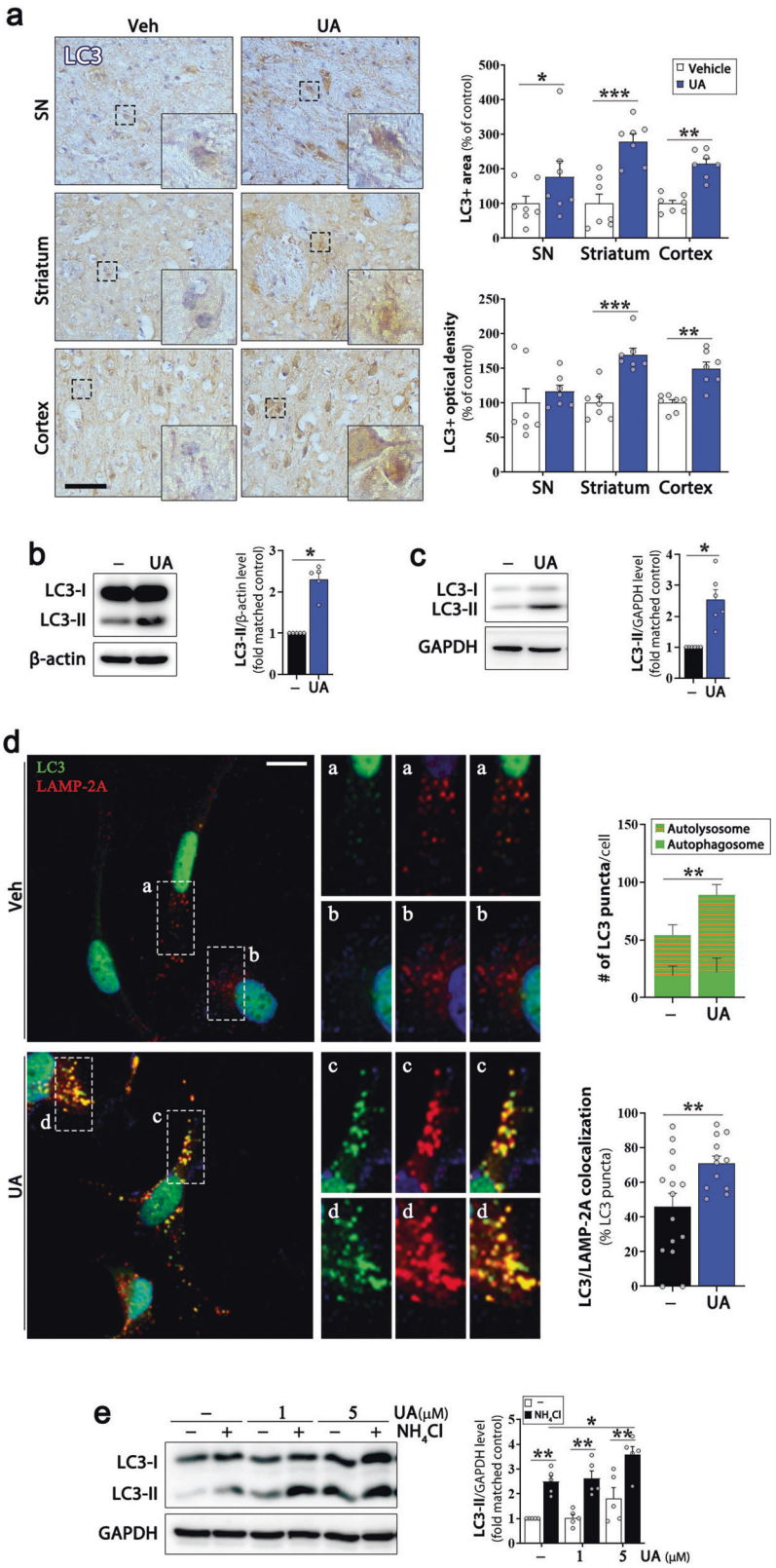

those neuronal cells. These results were further confirmed in 6-hydroxydopamine-treated SH-SY5Y cells, a widely used in vitro PD model [37], by evaluating βIII tubulin immunoreactivity (Fig. 7c) and lactate dehydrogenase activity (Fig. 7d). Similar to the results in rotenone-treated cells, both SP600125 and 3-MA interfered with the neuroprotective activity of UA in 6-hydroxydopamine-treated SH-SY5Y cells. Altogether, these results indicate that UA exhibits neuroprotective effects against PD-associated neuronal loss by activating JNK-dependent autophagy.

Fig. 4 Effect of ursolic acid (UA) on autophagy in neuronal cells. a Immunostaining for LC3 in the substantia nigra (SN), striatum, and cortex of mouse brains injected with rotenone with or without UA for 2 weeks; scale bar = 50 μm. Right, quantification of LC3-positive area and optical density; $n = 7$; two-way ANOVA followed by the post hoc Holm–Sidak test. **b** Immunoblotting for LC3 protein levels in primary cortical neurons treated with 5 μM UA for 16 h. Right, quantification of the LC3-II/β-actin protein levels; $n = 5$; Wilcoxon matched-pairs signed rank test. **c** Immunoblotting for LC3 protein levels in SH-SY5Y cells treated with 5 μM UA for 16 h. Right, quantification of the LC3-II/GAPDH protein levels; $n = 6$; Wilcoxon matched-pairs signed rank test. **d** Immunofluorescence staining of LC3 and LAMP-2A as in (**c**) scale bar = 20 μm. Right top, quantification of the number of LC3-positive spots that colocalized with (autophagosome) or without (autolysosome) LAMP-2A-labeled lysosomes per cell. Right bottom, percentage of LC3-positive spots that colocalized with LAMP-2A; $n = 13$; unpaired t test. **e** Immunoblotting for LC3 protein levels of the same cells as in (**c**) with or without 2 mM NH_4Cl. Right, quantification of the LC3-II/GAPDH protein levels; $n = 5$; two-way ANOVA followed by the post hoc Holm–Sidak test. The paired images were obtained at the same gain and offset settings. Data are expressed as mean ± SEM. $^*P < 0.05$; $^{**}P < 0.01$; $^{***}P < 0.001$. Veh vehicle.

DISCUSSION

In this study, we identified two novel findings regarding the potential use of UA to manage PD: (1) UA enhances the clearance of protein aggregates from the brain by the induction of autophagy, and (2) UA alleviates not only motor deficits but also prodromal non-motor signs in rotenone-induced PD mice. These results suggest that UA, as a supplement, may prevent neurodegeneration by regulating abnormal protein accumulation in the brain and alleviating disease progression from the prodromal stage before the onset of the characteristic motor symptoms of PD.

The age-related accumulation of misfolded and aggregated protein deposits such as Aβ and α-synuclein can be detected before the onset of characteristic symptoms and is a pathological hallmark of several neurodegenerative diseases [38]. Despite numerous studies and clinical trials, protein deposit-targeting drugs have not yet been approved by the Food and Drug Administration for neurodegenerative diseases. In this study, we showed that UA reduced p62 and ubiquitin deposits in the cortex, SNpc, and striatum of rotenone-treated mice (Fig. 3). The crucial role of UA in autophagy-mediated protein clearance and neuroprotection was verified in primary neuronal cells and differentiated SH-SY5Y cells; UA attenuated the accumulation of insoluble p62 and ubiquitin in rotenone- or MG132-treated cells, and increased the viability of cells treated with 6-hydroxydopamine or rotenone (Figs. 3, 7).

Autophagy is one of the main routes for the intracellular degradation of protein inclusions and has a pivotal role in neuronal proteostasis. Emerging evidence implicates the pathological relevance of autophagic flux dysregulation in neurodegenerative diseases, including PD. Postmortem studies have reported the accumulation of autophagic vacuoles and lysosomal depletion in the SN region of Patients with PD [39]. Furthermore, impaired autophagy-related regulators, such as the transcription factor EB, a major regulator of the autophagy-lysosome pathway, and transmembrane protein 175, the lysosomal K^+ channel, result in α-synuclein toxicity and PD pathogenesis [40]. Therapeutic approaches for PD that aim to increase autophagic flux are of growing interest in preclinical models [41]. Interestingly, UA has demonstrated anticancer activity through the induction of autophagy in gastric cancer cells and hepatocytes [8, 42]. However, it is not clear whether UA activates autophagy in neurons or whether UA-induced autophagy mediates neuroprotective activity. Although the neuroprotective effects of UA have been reported in a rotenone-induced PD mice model, studies on UA as a therapeutic for neuronal disorders have mainly focused on its antioxidant and anti-inflammatory activities [12, 43]. UA not only suppresses the generation of reactive oxygen species, but also attenuates DNA fragmentation and apoptotic cell death in Aβ-treated PC12 cells [44, 45]. Furthermore, it improves neurological deficits in cerebral ischemia in mice by activating the Nrf2 pathway [46]. In this study, UA significantly induced autophagy in neuronal cells (Fig. 4). Since rotenone causes the accumulation of protein aggregates by inhibiting autophagic flux prior to inducing cell death [32], it can function as an appropriate agent for analyzing the effects of autophagy-inducing drugs on the pathophysiology of PD. Our findings indicated that UA significantly reduced protein aggregates in the brain of rotenone-treated mice by facilitating the complete process of autophagy from the initial state of autophagosome formation to the subsequent turnover state of autophagic flux (Fig. 4). Moreover, UA improved the PD-like pathology and symptoms in the PD mice model; it attenuated DAergic neuronal loss in the SNpc and ameliorated motor dysfunction and prodromal non-motor symptoms. Additionally, the JNK inhibitor SP600125 or PI3K inhibitor 3-MA not only inhibited the induction of UA-induced autophagy, but also interfered with the neuroprotective effect of UA against neurotoxins, suggesting that UA possibly exhibits its neuroprotective activity by inducing autophagy.

In the initial stage of autophagy, the mTOR pathway and the class III-PI3K pathway are mainly involved in PAS formation [34]. mTORC1 is activated by diverse signals, including amino acids, growth factors, and calcium, and it negatively regulates autophagy. AMPK activation enhances autophagy via the direct activation of ULK1 or the indirect regulation of ULK1 through the suppression of mTORC1 [47]. In this study, p-mTOR levels were not altered by UA treatment at the early time points (1, 2, and 4 h; Fig. 6a), when LC3-II levels were significantly increased. These results suggest that the mTOR pathway is not directly responsible for UA-induced autophagy activation. Instead, UA activates autophagy through the JNK–Beclin 1–PI3KC3 signaling pathway, which is associated with upstream regulatory components of PAS formation for autophagy initiation [34]. The activation of JNK following starvation or proteasome inhibition results in the phosphorylation of Bcl-2 at multiple sites (Thr-69, Ser-70, and Ser-87), which interferes with its binding to Beclin 1, thus inducing autophagosome formation [34]. In this study, UA significantly increased p-JNK levels and resulted in Beclin 1 dissociation from Bcl-2 to promote autophagy (Figs. 6b, c, 7e). Consistent with this finding, the JNK inhibitor SP600125 inhibited the UA-mediated induction of autophagy and neuroprotection against neurotoxins (Figs. 6e, 7). Substantial evidence has demonstrated that UA induces cell death by activating JNK, which has been frequently observed in cancer cells, including hormone-refractory PC-3 prostate cancer cells [48], colorectal cancer cells [49], leukemia K562 cells [50], and glioblastoma multiforme cells [51]. However, the working concentration of UA for therapeutic effects in neurons is quite low compared with that for cancer cells.

In the present study, UA improved not only the motor deficits but also the depressive behavior of rotenone-treated mice (Fig. 1). It is encouraging that there is growing interest in the therapeutic potential of UA to attenuate motor and cognitive dysfunction [11] and protect dopaminergic neurons [12] in the rotenone-induced mouse model of PD. However, most of the studies reporting the protective effects of UA are still focused on its ability to regulate oxidative damage, excessive inflammation, and mitochondrial biogenesis. PD is accompanied by several non-motor symptoms, including olfactory loss, cognitive decline, depression, and anxiety, which frequently appear in the early stages of the disease [52, 53] and have a significant impact on the quality of life of Patients with PD. Attempts to develop a therapeutic approach based on pathology studies for the various non-motor symptoms in PD have increased significantly in recent years. However, treatment options are still

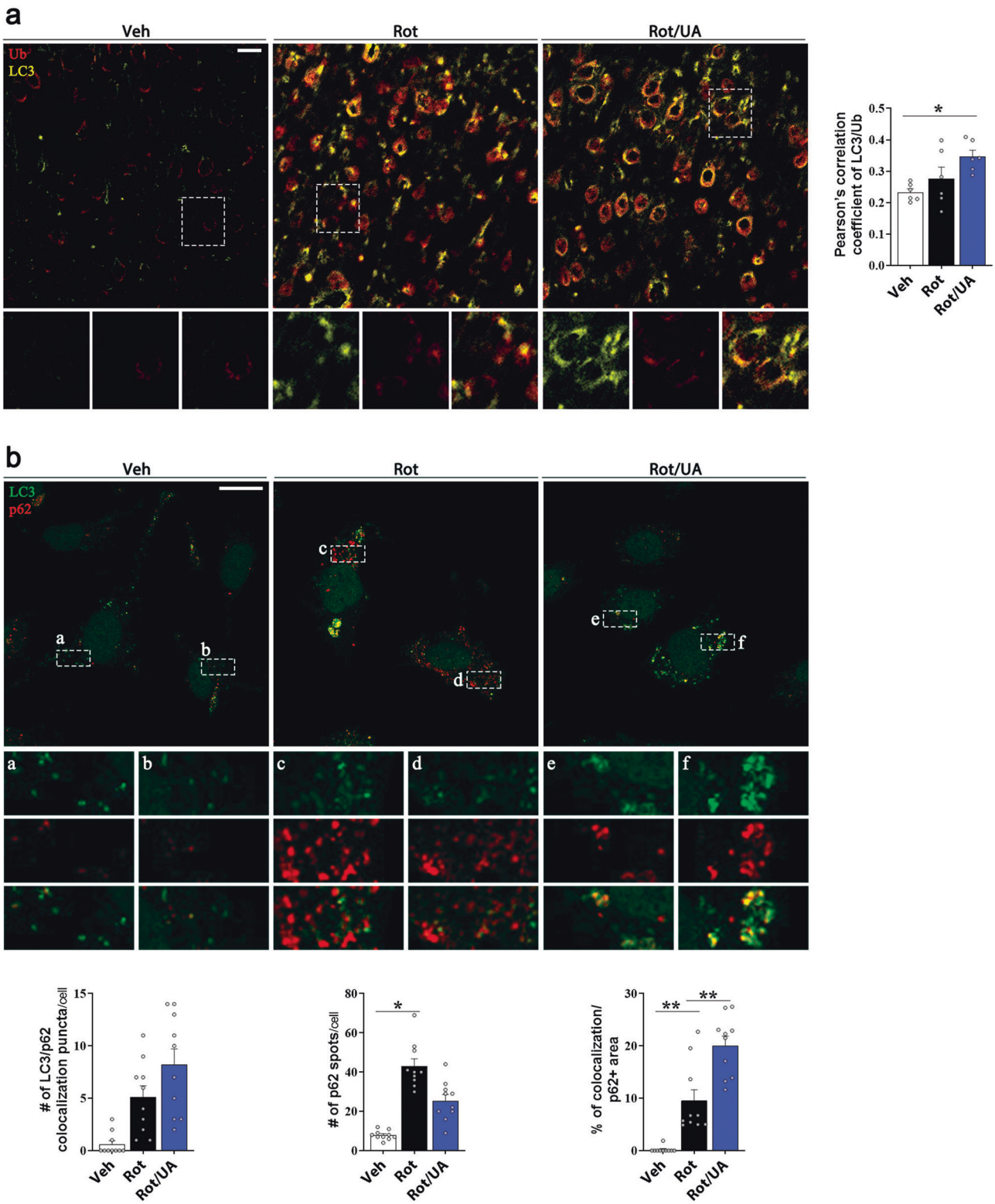

Fig. 5 Effect of ursolic acid (UA) on the co-localization of LC3 and p62 protein inclusions. a Immunofluorescence staining of LC3 and ubiquitin in the cortex of mouse brains injected with rotenone with or without UA for 2 weeks; scale bar = 20 μm. Right, quantification of LC3 overlapped with ubiquitin using the Pearson's correlation coefficient. **b** Immunofluorescence staining of LC3 and p62 in SH-SY5Y cells treated with 2 μM rotenone and/or 5 μM UA for 6 h. Bottom left, quantification of the number of colocalized spots per cell; scale bar = 20 μm. Bottom right, quantification of the mean size of the colocalized spots per cell; $n = 10–16$; one-way ANOVA followed by the post hoc Holm–Sidak test. The paired images were obtained at the same gain and offset settings. Data are expressed as mean ± SEM. $^{*}P < 0.05$; $^{**}P < 0.01$. Rot rotenone, Ub ubiquitin, Veh vehicle.

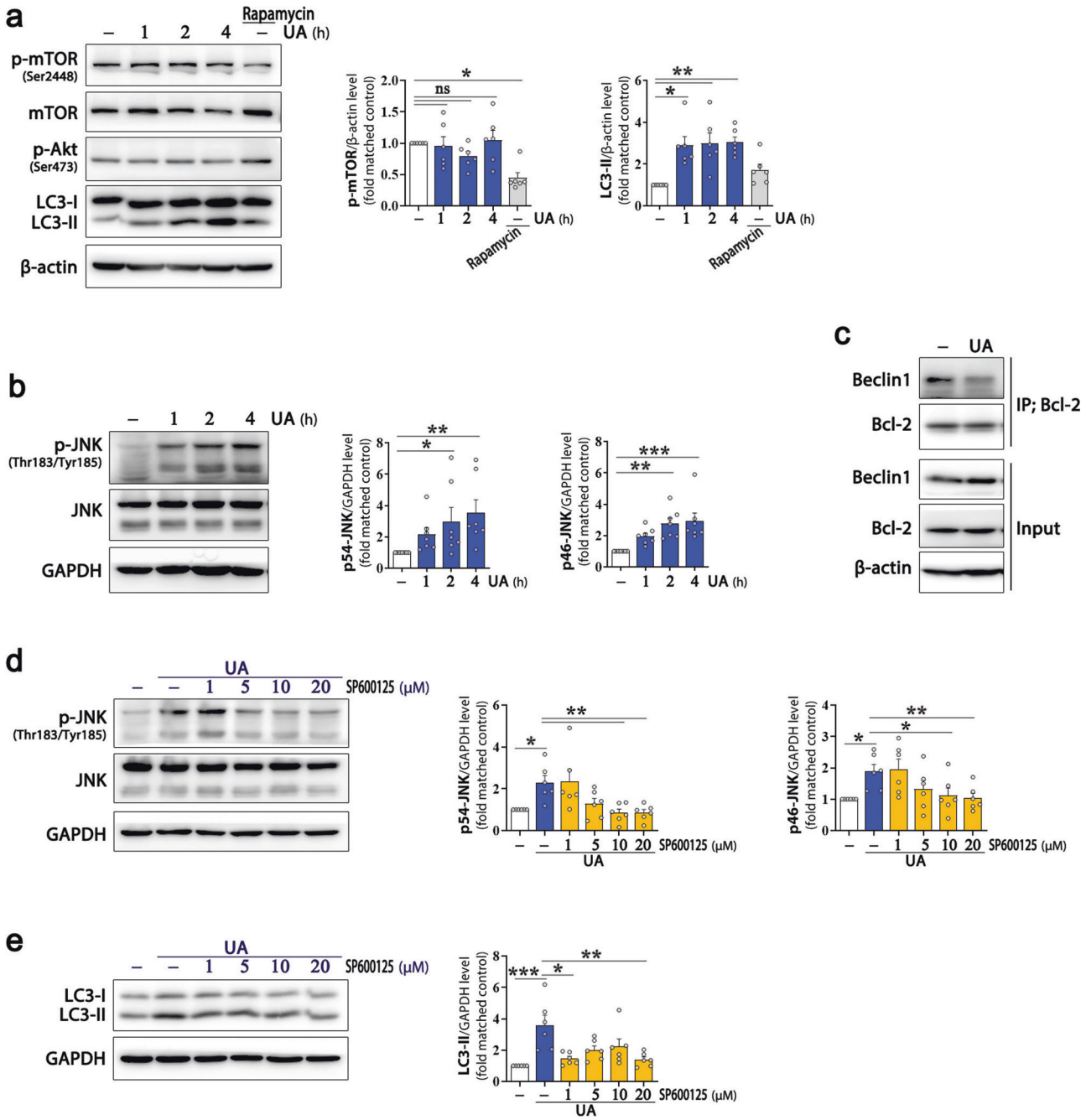

Fig. 6 Involvement of the JNK pathway in ursolic acid (UA)-induced autophagy. a Immunoblotting for p-mTOR (Ser2448), mTOR, p-Akt (Ser473), and LC3 protein levels in SH-SY5Y cells treated with 5 μM UA for 1, 2, and 4 h or 2.5 μM rapamycin for 4 h. Right, quantification of the p-mTOR (Ser2448) and LC3-II/GAPDH protein levels; $n = 6$; one-way ANOVA followed by the post hoc Dunn's multiple comparisons test. **b** Immunoblotting for p-JNK (Thr183/Tyr185) and JNK protein levels in the same cells as in (**a**). Right, quantification of the p54-JNK or p46-JNK/GAPDH protein levels; $n = 7$; one-way ANOVA followed by the post hoc Dunn's multiple comparisons test. **c** Immunoblotting for Bcl-2 and Beclin 1 based on total protein (input) and immunoprecipitation with a Bcl-2 antibody in SH-SY5Y cells treated with 5 μM UA for 4 h. **d** Immunoblotting for p-JNK (Thr183/Tyr185) and JNK protein levels in SH-SY5Y cells treated with 5 μM UA for 4 h followed by 1 h of incubation with or without 1, 5, 10, or 20 μM SP600125. Right, quantification of the p54-JNK or p46-JNK/GAPDH protein levels; $n = 6$; one-way ANOVA followed by the post hoc Dunn's multiple comparisons test. **e** Immunoblotting for LC3 protein levels with 5 μM UA for 16 h as in (**d**). Right, quantification of the LC3-II/GAPDH protein levels; $n = 6$; one-way ANOVA followed by the post hoc Dunn's multiple comparisons test. Data are expressed as mean ± SEM. $^*P < 0.05$; $^{**}P < 0.01$; $^{***}P < 0.001$. ns not significant. IP immunoprecipitation.

limited; drugs used clinically for Patients with PD mainly provide symptomatic relief of motor deficits by increasing DA signaling, which is not associated with significant improvement of non-motor symptoms. Although the pathogenesis of non-motor symptoms in PD has not been fully elucidated, recent evidence suggests that it could be associated with an increased accumulation of protein deposits in the brain at a very early stage. Misfolded α-synuclein in the peripheral tissue propagates and progresses toward the brain at an early stage and could result in the prodromal non-motor symptoms [54, 55]. Moreover, amygdaloid α-synucleinopathy has been associated with non-motor symptoms such as olfactory dysfunction and depression in PD [56]. Small HSP27 was shown to

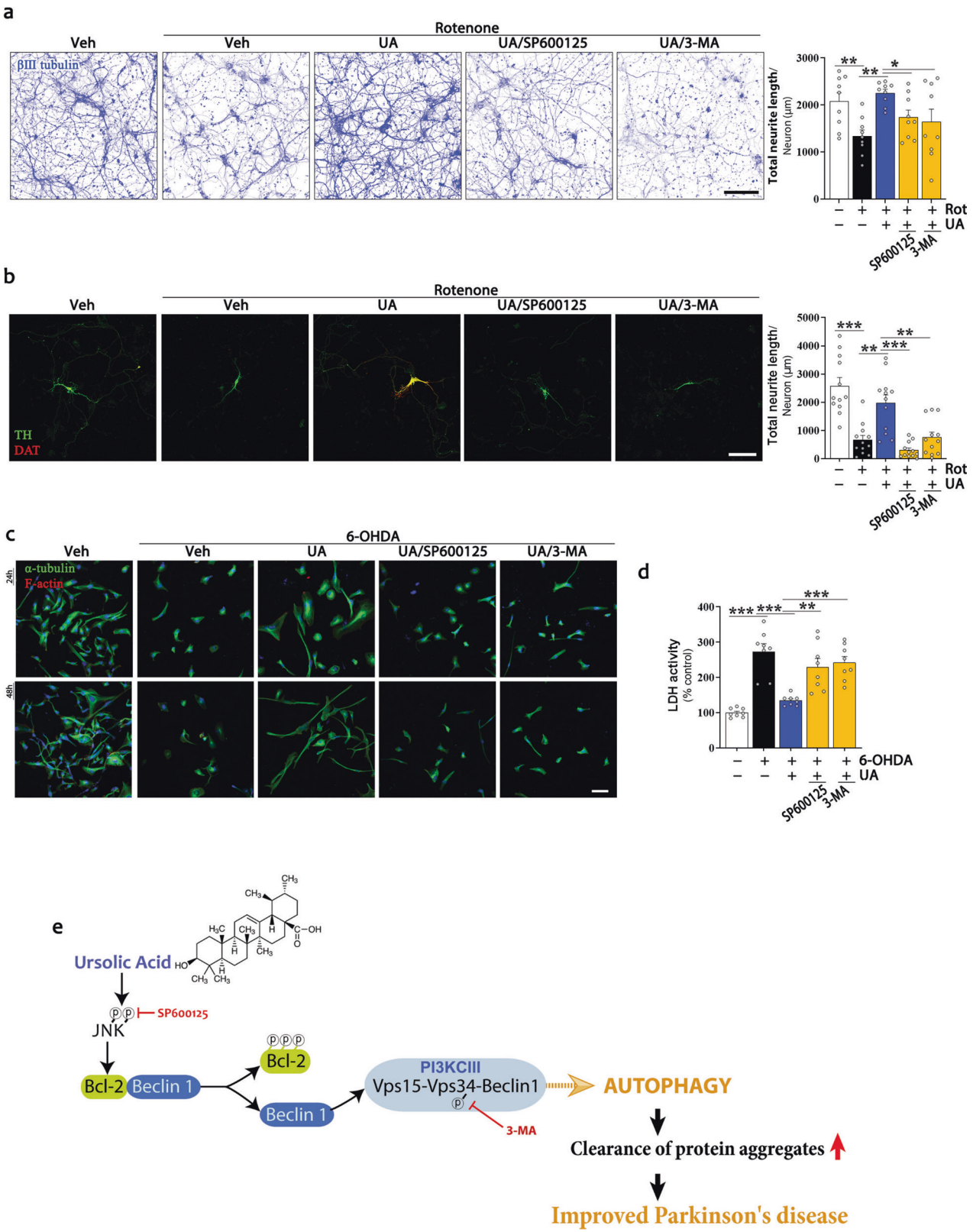

reduce α-synuclein aggregation and may prevent or delay the non-motor symptoms of PD [57]. In our previous study, we demonstrated the association of non-motor symptoms in rotenone-treated mice with the accumulation of protein aggregates in the brain, and therefore, autophagy inducers could be effective for the regulation of PD progression from the prodromal stage [32]. From this perspective, our present results showing that UA ameliorates non-motor signs in a PD mice model has important clinical implications. Numerous studies are being conducted on the potential of natural compounds as therapeutic agents for neurodegenerative diseases. Although the clinical application of UA in the prevention and treatment of PD requires further studies, including improving its

Fig. 7 Involvement of the JNK pathway in the neuroprotective activity of ursolic acid (UA). a Immunofluorescence staining of βIII tubulin in primary cortical neurons treated with 5 nM rotenone and 5 μM UA for 2 days followed by 1 h of incubation with or without 10 μM SP600125 or 3-MA; scale bar = 100 μm. Right, quantitation of total neurite length of βIII tubulin-positive neurons; $n = 9$. **b** Immunofluorescence staining of TH and DA transporter (DAT) in dopaminergic primary neurons treated in the same manner as in (**a**); scale bar = 100 μm. Right, quantitation of total neurite length of TH-positive neurons; $n = 12$. **c**, **d** Immunofluorescence staining of α-tubulin and F-actin (**c**) and lactate dehydrogenase assays (**d**) in SH-SY5Y cells treated with 100 μM 6-OHDA and 5 μM UA with or without 10 μM SP600125 or 3-MA; scale bar = 100 μm. **e** Schematic representation of the mechanism involved in UA-induced autophagy. UA phosphorylates JNK followed by Bcl-2 phosphorylation. The activation of Beclin 1 mediated by dissociation from Bcl-2 enhances the formation of PI3KCIII and initiates autophagosome formation for clearance of protein aggregates; one-way ANOVA followed by the post hoc Holm–Sidak test. The paired images were obtained at the same gain and offset settings. Data are expressed as mean ± SEM. $^{*}P < 0.05$; $^{**}P < 0.01$; $^{***}P < 0.001$. LDH lactate dehydrogenase, 3-MA 3-methyladenine, TH tyrosine hydroxylase, DA dopamine, Veh vehicle, Rot rotenone.

bioavailability in the brain, validation of the effective dose, and a long-term safety evaluation, our current findings demonstrating that UA induces the autophagic clearance of protein aggregates and attenuates PD-like non-motor and motor signs provide experimental evidence that UA could be a potential candidate for developing PD therapeutics.

ACKNOWLEDGEMENTS

This work was supported by the GRRC program of Gyeonggi Province, Korea (GRRC-CHA2017-A01, Validity and Safety Evaluation of Regional Specialized Resources) and the Basic Science Research Program through the National Research Foundation of Korea funded by the Ministry of Science, ICT & Future Planning, Korea (NRF-2016R1C1B1015991, NRF-2019R1H1A1080255, and NRF2021R1A2C1013180).

AUTHOR CONTRIBUTIONS

YB, KJ, and HJC conceptualized and designed the study. YB, YK, MK, and SHM performed in vivo and in vitro experiments. YB, YK, MK, SHM, and HJC performed the data analysis and interpretation. YB and HJC wrote the original paper draft and obtained research funding. All authors have read and approved the final paper.

ADDITIONAL INFORMATION

Supplementary information The online version contains supplementary material available at https://doi.org/10.1038/s41401-022-00988-2.

Competing interests: The authors declare no competing interests.

Ethics approval: All animal care and experimental procedures complied with and were approved by the Institutional Animal Care and Use Committee (IACUC) of CHA University (IACUC190113, IACUC200111, and IACUC210106). The animal studies are reported in compliance with the ARRIVE guidelines [58]. Every effort was made to minimize animal suffering and to perform the experiments using fewer mice.

REFERENCES

1. Kumar V, Sami N, Kashav T, Islam A, Ahmad F, Hassan MI. Protein aggregation and neurodegenerative diseases: From theory to therapy. Eur J Med Chem. 2016;124:1105–20.
2. Li J, Zhang L, Jiang Z, Shu B, Li F, Bao Q. Toxicities of aristolochic acid I and aristololactam I in cultured renal epithelial cells. Toxicol In Vitro. 2010;24:1092–7.
3. Lim J, Bang Y, Choi HJ. Abnormal hippocampal neurogenesis in Parkinson's disease: relevance to a new therapeutic target for depression with Parkinson's disease. Arch Pharm Res. 2018;41:943–54.
4. Funderburk SF, Wang QJ, Yue Z. The Beclin 1-VPS34 complex–at the crossroads of autophagy and beyond. Trends Cell Biol. 2010;20:355–62.
5. Yan H, Gao Y, Zhang Y. Inhibition of JNK suppresses autophagy and attenuates insulin resistance in a rat model of nonalcoholic fatty liver disease. Mol Med Rep. 2017;15:180–6.
6. Lu J, Zheng YL, Wu DM, Luo L, Sun DX, Shan Q. Ursolic acid ameliorates cognition deficits and attenuates oxidative damage in the brain of senescent mice induced by D-galactose. Biochem Pharmacol. 2007;74:1078–90.
7. Lin CW, Chin HK, Lee SL, Chiu CF, Chung JG, Lin ZY, et al. Ursolic acid induces apoptosis and autophagy in oral cancer cells. Environ Toxicol. 2019;34:983–91.
8. Leng S, Iwanowycz S, Saaoud F, Wang J, Wang Y, Sergin I, et al. Ursolic acid enhances macrophage autophagy and attenuates atherogenesis. J Lipid Res. 2016;57:1006–16.
9. Wu J, Zhao S, Tang Q, Zheng F, Chen Y, Yang L, et al. Activation of SAPK/JNK mediated the inhibition and reciprocal interaction of DNA methyltransferase 1 and EZH2 by ursolic acid in human lung cancer cells. J Exp Clin Cancer Res. 2015;34:99.
10. Katashima CK, Silva VR, Gomes TL, Pichard C, Pimentel GD. Ursolic acid and mechanisms of actions on adipose and muscle tissue: a systematic review. Obes Rev. 2017;18:700–11.
11. Peshattiwar V, Muke S, Kaikini A, Bagle S, Dighe V, Sathaye S. Mechanistic evaluation of Ursolic acid against rotenone induced Parkinson's disease- emphasizing the role of mitochondrial biogenesis. Brain Res Bull. 2020;160:150–61.
12. Zahra W, Rai SN, Birla H, Singh SS, Rathore AS, Dilnashin H, et al. Neuroprotection of rotenone-induced Parkinsonism by ursolic acid in PD mouse model. CNS Neurol Disord Drug Targets. 2020;19:527–40.
13. Seo DY, Lee SR, Heo JW, No MH, Rhee BD, Ko KS, et al. Ursolic acid in health and disease. Korean J Physiol Pharmacol. 2018;22:235–48.
14. Rai SN, Yadav SK, Singh D, Singh SP. Ursolic acid attenuates oxidative stress in nigrostriatal tissue and improves neurobehavioral activity in MPTP-induced Parkinsonian mouse model. J Chem Neuroanat. 2016;71:41–9.
15. Li Y, Liu W, Oo TF, Wang L, Tang Y, Jackson-Lewis V, et al. Mutant LRRK2(R1441G) BAC transgenic mice recapitulate cardinal features of Parkinson's disease. Nat Neurosci. 2009;12:826–8.
16. Walsh RN, Cummins RA. The Open-Field Test: a critical review. Psychol Bull. 1976;83:482–504.
17. Francardo V, Recchia A, Popovic N, Andersson D, Nissbrandt H, Cenci MA. Impact of the lesion procedure on the profiles of motor impairment and molecular responsiveness to *L*-DOPA in the 6-hydroxydopamine mouse model of Parkinson's disease. Neurobiol Dis. 2011;42:327–40.
18. Castagné V, Moser PC, Porsolt RD. Preclinical behavioral models for predicting antipsychotic activity. Adv Pharmacol. 2009;57:381–418.
19. Sadleir KR, Kandalepas PC, Buggia-Prévot V, Nicholson DA, Thinakaran G, Vassar R. Presynaptic dystrophic neurites surrounding amyloid plaques are sites of microtubule disruption, BACE1 elevation, and increased Aβ generation in Alzheimer's disease. Acta Neuropathol. 2016;132:235–56.
20. Bang Y, Lim J, Kim SS, Jeong HM, Jung KK, Kang IH, et al. Aroclor1254 interferes with estrogen receptor-mediated neuroprotection against beta-amyloid toxicity in cholinergic SN56 cells. Neurochem Int. 2011;59:582–90.
21. Kwon Y, Bang Y, Moon SH, Kim A, Choi HJ. Amitriptyline interferes with autophagy-mediated clearance of protein aggregates via inhibiting autophagosome maturation in neuronal cells. Cell Death Dis. 2020;11:874.
22. Cannon JR, Tapias V, Na HM, Honick AS, Drolet RE, Greenamyre JT. A highly reproducible rotenone model of Parkinson's disease. Neurobiol Dis. 2009;34:279–90.
23. Johnson ME, Bobrovskaya L. An update on the rotenone models of Parkinson's disease: their ability to reproduce the features of clinical disease and model gene-environment interactions. Neurotoxicology. 2015;46:101–16.
24. Moon SH, Kwon Y, Huh YE, Choi HJ. Trehalose ameliorates prodromal non-motor deficits and aberrant protein accumulation in a rotenone-induced mouse model of Parkinson's disease. Arch Pharm Res. 2022;45:417–32.
25. Ross CA, Poirier MA. Protein aggregation and neurodegenerative disease. Nat Med. 2004;10 Suppl:S10–7.
26. Kuusisto E, Kauppinen T, Alafuzoff I. Use of p62/SQSTM1 antibodies for neuropathological diagnosis. Neuropathol Appl Neurobiol. 2008;34:169–80.
27. Bang Y, Kang BY, Choi HJ. Preconditioning stimulus of proteasome inhibitor enhances aggresome formation and autophagy in differentiated SH-SY5Y cells. Neurosci Lett. 2014;566C:263–8.
28. Bang Y, Kim KS, Seol W, Choi HJ. LRRK2 interferes with aggresome formation for autophagic clearance. Mol Cell Neurosci. 2016;75:71–80.
29. Hart PD, Young MR. Ammonium chloride, an inhibitor of phagosome-lysosome fusion in macrophages, concurrently induces phagosome-endosome fusion, and opens a novel pathway: studies of a pathogenic mycobacterium and a non-pathogenic yeast. J Exp Med. 1991;174:881–9.

30. Xiong N, Xiong J, Jia M, Liu L, Zhang X, Chen Z, et al. The role of autophagy in Parkinson's disease: rotenone-based modeling. Behav Brain Funct. 2013;9:13.
31. Wu F, Xu HD, Guan JJ, Hou YS, Gu JH, Zhen XC, et al. Rotenone impairs autophagic flux and lysosomal functions in Parkinson's disease. Neuroscience. 2015;284:900–11.
32. Mader BJ, Pivtoraiko VN, Flippo HM, Klocke BJ, Roth KA, Mangieri LR, et al. Rotenone inhibits autophagic flux prior to inducing cell death. ACS Chem Neurosci. 2012;3:1063–72.
33. Sarkar S. Regulation of autophagy by mTOR-dependent and mTOR-independent pathways: autophagy dysfunction in neurodegenerative diseases and therapeutic application of autophagy enhancers. Biochem Soc Trans. 2013;41:1103–30.
34. Wei Y, Pattingre S, Sinha S, Bassik M, Levine B. JNK1-mediated phosphorylation of Bcl-2 regulates starvation-induced autophagy. Mol Cell. 2008;30:678–88.
35. He C, Zhu H, Li H, Zou MH, Xie Z. Dissociation of Bcl-2-Beclin1 complex by activated AMPK enhances cardiac autophagy and protects against cardiomyocyte apoptosis in diabetes. Diabetes. 2013;62:1270–81.
36. Wu YT, Tan HL, Shui G, Bauvy C, Huang Q, Wenk MR, et al. Dual role of 3-methyladenine in modulation of autophagy via different temporal patterns of inhibition on class I and III phosphoinositide 3-kinase. J Biol Chem. 2010; 285:10850–61.
37. Saito Y, Nishio K, Ogawa Y, Kinumi T, Yoshida Y, Masuo Y, et al. Molecular mechanisms of 6-hydroxydopamine-induced cytotoxicity in PC12 cells: involvement of hydrogen peroxide-dependent and -independent action. Free Radic Biol Med. 2007;42:675–85.
38. Braak H, Del Tredici K, Rüb U, de Vos RA, Jansen Steur EN, Braak E. Staging of brain pathology related to sporadic Parkinson's disease. Neurobiol Aging. 2003;24:197–211.
39. Dehay B, Bové J, Rodríguez-Muela N, Perier C, Recasens A, Boya P, et al. Pathogenic lysosomal depletion in Parkinson's disease. J Neurosci. 2010;30:12535–44.
40. Decressac M, Mattsson B, Weikop P, Lundblad M, Jakobsson J, Björklund A. TFEB-mediated autophagy rescues midbrain dopamine neurons from α-synuclein toxicity. Proc Natl Acad Sci USA. 2013;110:E1817–26.
41. Fowler AJ, Moussa CE. Activating autophagy as a therapeutic strategy for Parkinson's disease. CNS Drugs. 2018;32:1–11.
42. Leng S, Hao Y, Du D, Xie S, Hong L, Gu H, et al. Ursolic acid promotes cancer cell death by inducing Atg5-dependent autophagy. Int J Cancer. 2013;133:2781–90.
43. Habtemariam S. Antioxidant and anti-inflammatory mechanisms of neuroprotection by ursolic acid: addressing brain injury, cerebral ischemia, cognition deficit, anxiety, and depression. Oxid Med Cell Longev. 2019;2019:8512048.
44. Heo HJ, Cho HY, Hong B, Kim HK, Heo TR, Kim EK, et al. Ursolic acid of Origanum majorana L. reduces Abeta-induced oxidative injury. Mol Cells. 2002;13:5–11.
45. Hong SY, Jeong WS, Jun M. Protective effects of the key compounds isolated from Corni fructus against β-amyloid-induced neurotoxicity in PC12 cells. Molecules. 2012;17:10831–45.
46. Li L, Zhang X, Cui L, Wang L, Liu H, Ji H, et al. Ursolic acid promotes the neuroprotection by activating Nrf2 pathway after cerebral ischemia in mice. Brain Res. 2013;1497:32–9.
47. Hardie DG. AMPK and autophagy get connected. EMBO J. 2011;30:634–5.
48. Zhang Y, Kong C, Zeng Y, Wang L, Li Z, Wang H, et al. Ursolic acid induces PC-3 cell apoptosis via activation of JNK and inhibition of Akt pathways in vitro. Mol Carcinog. 2010;49:374–85.
49. Xavier CP, Lima CF, Pedro DF, Wilson JM, Kristiansen K, Pereira-Wilson C. Ursolic acid induces cell death and modulates autophagy through JNK pathway in apoptosis-resistant colorectal cancer cells. J Nutr Biochem. 2013;24:706–12.
50. Liu XS, Jiang J. Induction of apoptosis and regulation of the MAPK pathway by ursolic acid in human leukemia K562 cells. Planta Med. 2007;73:1192–4.
51. Conway GE, Zizyte D, Mondala JRM, He Z, Lynam L, Lecourt M, et al. Ursolic acid inhibits collective cell migration and promotes JNK-dependent lysosomal associated cell death in glioblastoma multiforme cells. Pharmaceuticals. 2021;14:91–106.
52. Bang Y, Lim J, Choi HJ. Recent advances in the pathology of prodromal non-motor symptoms olfactory deficit and depression in Parkinson's disease: clues to early diagnosis and effective treatment. Arch Pharm Res. 2021;44:588–604.
53. Lim J, Kim HI, Bang Y, Choi HJ. Peroxisome proliferator-activated receptor gamma: a novel therapeutic target for cognitive impairment and mood disorders that functions via the regulation of adult neurogenesis. Arch Pharm Res. 2021;44:553–63.
54. Manfredsson FP, Luk KC, Benskey MJ, Gezer A, Garcia J, Kuhn NC, et al. Induction of alpha-synuclein pathology in the enteric nervous system of the rat and non-human primate results in gastrointestinal dysmotility and transient CNS pathology. Neurobiol Dis. 2018;112:106–18.
55. Ferreira N, Goncalves NP, Jan A, Jensen NM, van der Laan A, Mohseni S, et al. Trans-synaptic spreading of alpha-synuclein pathology through sensory afferents leads to sensory nerve degeneration and neuropathic pain. Acta Neuropathol Commun. 2021;9:31.
56. Flores-Cuadrado A, Ubeda-Banon I, Saiz-Sanchez D, de la Rosa-Prieto C, Martinez-Marcos A. alpha-Synuclein staging in the amygdala of a Parkinson's disease model: cell types involved. Eur J Neurosci. 2015;41:137–46.
57. Navarro-Zaragoza J, Cuenca-Bermejo L, Almela P, Laorden ML, Herrero MT. Could small heat shock protein HSP27 be a first-line target for preventing protein aggregation in Parkinson's disease? Int J Mol Sci. 2021;22:3038–50.
58. Percie du Sert N, Hurst V, Ahluwalia A, Alam S, Avey MT, Baker M, et al. The ARRIVE guidelines 2.0: updated guidelines for reporting animal research. BMJ Open Sci. 2020;4:e100115.